ROZPRAWY INŻYNIERSKIE • ENGINEERING TRANSACTIONS •30, 3-4, 327—353, 1982
Polska Akademia Nauk • Instytut Podstawowych Problemów Techniki

SOME RESULTS IN THE NUMERICAL ANALYSIS OF STRUCTURAL INSTABILITIES
PART I. STATICS

M. KLEIBER (WARSZAWA)

Some problems of nonlinear structural statics are dealt with in the paper. Attention is restricted to numerical analyses carried out by means of the finite element method. The paper contains a short discussion of the static stability problem which is followed by a number of numerical examples.

1. Introduction

The purpose of static stability analysis is to supply some important information about the structural behaviour in the vicinity of critical points on the primary equilibrium path. Such an analysis is aimed at both quantitative and qualitative estimates derivable at a significant reduction in cost, as compared with a detailed numerical study of the structural behaviour in the whole external loading range of interest. Static stability analysis is particularly helpful at the preliminary design stage when the analyst must rely on design charts for simple model structures. For final design the analyst can then use the refined nonlinear analysis programs, the effective use of which is strongly dependent on a general understanding of the basic buckling phenomena of the model structure. The above is valid for both elastic and inelastic structures. However, bifurcation buckling analyses involving plasticity have so far been applied to simple structures with uniform prestress only. Nevertheless, basis conceptual difficulties have been cleared up so that now it is widely understood that the complicated nature of the plastic flow does not preclude the use of bifurcation buckling analysis to predict instability failure of practical structures ([1]). The fact that the collapse load is only slightly above the bifurcation load for vanishingly small imperfections makes elasto-plastic bifurcation analysis in principle just as suitable for design purposes as elastic bifurcation analysis.

There is a great number of structures for wich either elastic or, at the other extreme, rigid-plastic material models can supply interesting information as to their ultimate critical behaviour. However, there exist also situations in which a complete elasto-inelastic model is the only appropriate one to analyse buckling phenomena in the whole load range of interest. To illustrate the need for such an analysis, we could cite two structures discussed throughly in [4]. In Figs. 1 and 2

([1]) The reader is referred to [1–3] for a detailed explanation and further comments on this subject.

the elastic and plastic zones are shown as derived numerically, corresponding to the static pre- and postcritical load levels. It is seen that both purely elastic and rigid-plastic material models could be inadequate for buckling load estimation. In both examples the plastic zones played an obviously important role in the calculation process while the elastic zones had a great influence upon the structures prebuckling shape, thus contributing significantly to the buckling loads calculated.

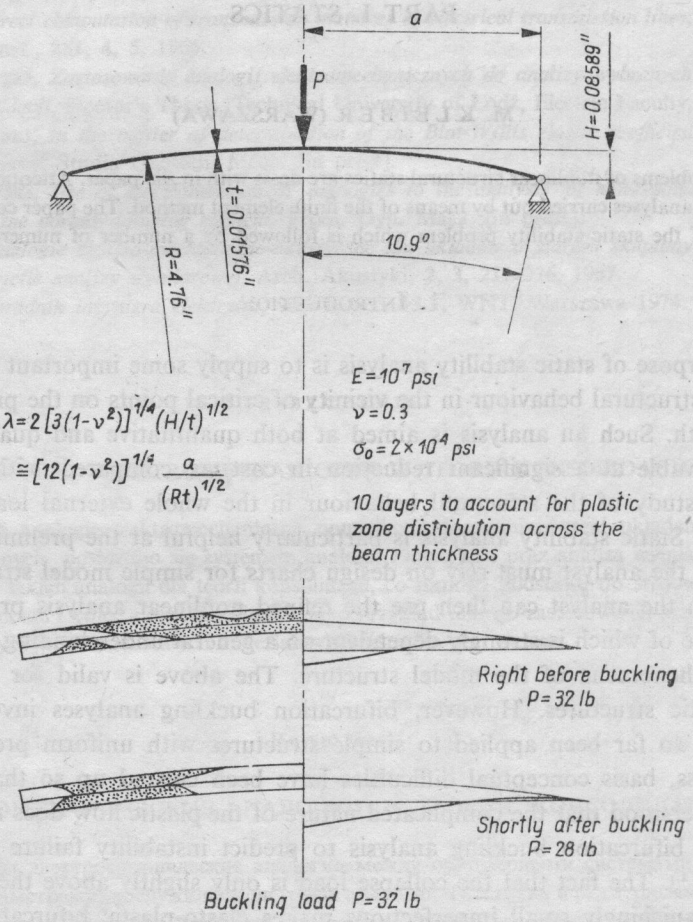

FIG. 1. Progression of plastic zones and deflection profiles.

Buckling analysis becomes by far more complex when we pass to the transient problems. It is by no means obvious that the fruitful concepts of static buckling can also be taken advantage of in the domain of dynamic problems. Inclusion of time as an additional parameter complicates matters considerably. It can be said in general that the determination of dynamic buckling loads for structures is still not a very developed area, even with regard to the definition of reasonable failure

criteria(2). Nonlinear dynamic stability solutions available in the literature for curved structures are very limited in scope; most are confined to symmetric analysis under ideal impulse loadings often within a one degree-of-freedom approximation. The extent to which designers can safely use either of these idealized dynamic so-

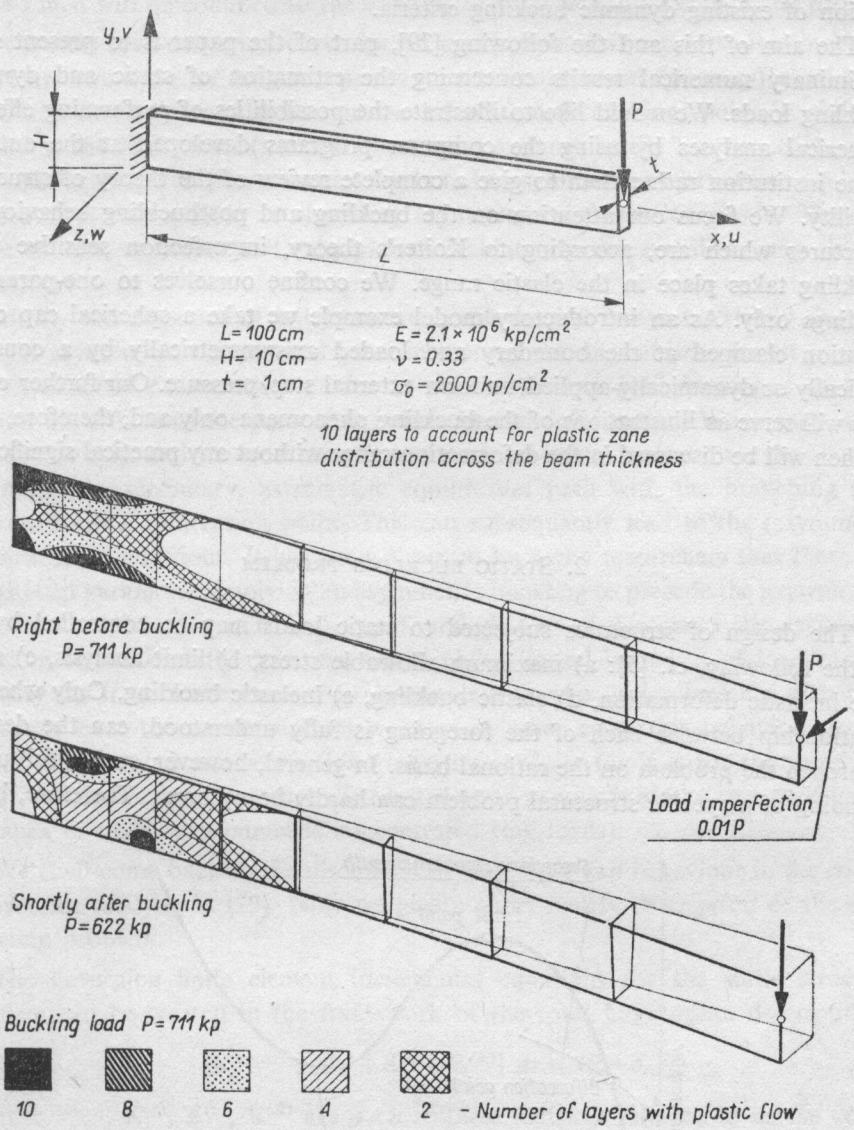

FIG. 2. Progression of plastic zones and deflection profiles.

(2) We note at this place that the fruitful Lyapunow concept of direct stability analysis is not very useful in practice as it concerns the analysis in the infinite time domain, considers the initial disturbances of the motion only and assumes certain smoothness conditions which are often difficult to satisfy. The applications of this approach have so far been restricted to rather simple elastic problems.

lutions or static solutions to determine realistic dynamic buckling loads requires clarification. A need exists, therefore, for a thorough exploration of representative problems dealing with some characteristic structures which will shed light on the understanding of dynamic buckling behaviour in general and will lead to the evaluation of existing dynamic buckling criteria.

The aim of this and the following [29], part of the paper is to present some preliminary numerical results concerning the estimation of static and dynamic buckling loads. We would like to illustrate the possibilities of performing effective numerical analyses by using the computer programs developed at the author's home institution rather than to give a complete review of the theory of structural stability. We focus our attention on the buckling and postbuckling behaviour of structures which are, according to Koiter's theory, imperfection sensitive when buckling takes place in the elastic range. We confine ourselves to one-parameter loadings only. As an introductory model example we take a spherical cap of revolution clamped at the boundary and loaded axisymmetrically by a constant, statically or dynamically-applied uniform external step pressure. Our further examples will serve as illustrations of the buckling phenomena only and, therefore, some of then will be discussed in the deformation range without any practical significance.

2. Static buckling problem

The design of structures subjected to static loads may be controlled by one of the following, cf. [5]: a) maximum allowable stress, b) limit analysis, c) excessive inelastic deformation, d) elastic buckling, e) inelastic buckling. Only when the relationship between each of the foregoing is fully understood, can the designer approach the problem on the rational basis. In general, however, such a full understanding of a specific structural problem can hardly be achieved. Therefore, basing

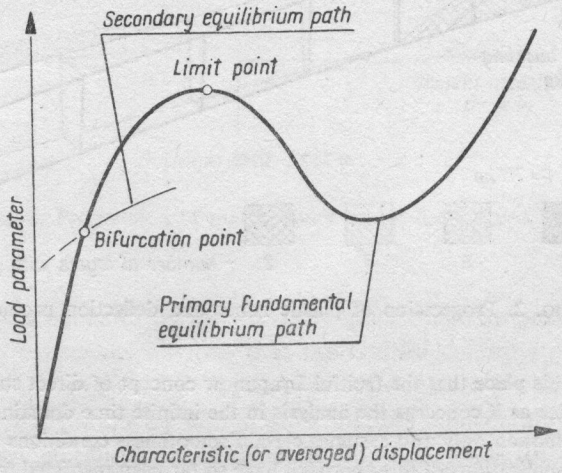

Fig. 3. Typical load-displacement curve for an elastic spherical cap.

upon our engineering intuition, we try to identify classes of problems in which a simplified method can be used supplying limited informations about some of the design factors only. As we shall see, some of our numerical analyses will aim at giving a full nonlinear description of the problem. There will, however, exist some which will be confined to the analysis of very limited aspects of the problem.

A typical load-deflection curve for an elastic spherical cap is shown in Fig. 3. There are two types of singular points on the fundamental (primary) equilibrium path. The first type is identified as the bifurcation (branching) point([3]) while the second as the limit point (point of the local maximum load). The branching point characterizes the situation in which the initial axisymmetric deformation mode can bifurcate into an (stable or unstable) asymmetric deformation mode. The limit point in turn corresponds to the loss of stability by the so-called snap through behaviour.

Ideally the response of axisymmetric shells loaded axisymmetrically does not contain asymmetric components because there is no mechanism present to excite the asymmetric deformation mode. In real structures (and loadings), however, natural imperfections are present to induce such a deformation. When such imperfections do exist and the load exceeds some critical value, it may force the structure to follow the secondary, asymmetric equilibrium path with the branching point referred to as a bifurcation point. This can subsequently lead to the (asymmetric) snap-through behaviour. It has been observed by many researchers that there exist critical cap parameters implying an asymmetric buckling to precede the axisymmetric snap-through. Moreover, it has been found that in certain cases the asymmetric buckling behavior of the spherical cap is characterized by a loss of load carrying capacity (as it is in the case of a clamped elastic cap under pressure distributed uniformly over the entire surface) whereas in other cases this behaviour can be characterized by an increase in load carrying capacity (as it is for the same shell under certain uniform pressure distributed over a region of the cap surrounding the apex or under axisymmetric concentrated ring loads).

We shall come back to the discussion of the elastic cap behaviour in the context of dynamic analysis in [29]. Now we give a short matrix description of the static buckling problem.

The governing finite element incremental equations for the static structural problem can be written in the framework of the total Lagrangean description as

$$[\mathbf{K}^{(\text{const})}+\mathbf{K}^{(\sigma)}+\mathbf{K}^{(u)}+\mathbf{K}^{(R)}]\,\Delta\mathbf{r}=\Delta\mathbf{R}-\mathbf{J}, \tag{2.1}$$

where $\mathbf{K}^{(\text{const})}$, $\mathbf{K}^{(\sigma)}$, $\mathbf{K}^{(u)}$, $\mathbf{K}^{(R)}$ are $n\times n$ stiffness matrices referred to as the constitutive, the initial stress, the initial displacement and the load matrix, respectively, n is the global number of the displacement-type degrees of freedom in the discretized structure, $\Delta\mathbf{r}$ is the vector of the incremental generalized displacement, $\Delta\mathbf{R}$ is the vector of the incremental external loading while $\mathbf{J}$ is the so-called initial load

([3]) As a matter of fact, in rotationally-symmetric spherical caps we observe the so-called asymmetric bifurcation points.

vector corresponding to nonequilibrated nodal forces resulting from accumulated errors of the numerical algorithm.

It is essential to note that the matrix $\mathbf{K}^{(\sigma)}$ is a linear and homogeneous function of the second Piola–Kirchhoff stress components S_{ij} while the matrix $\mathbf{K}^{(u)}$ consists of only the terms which are either quadratic or linear in the total displacement components. For a broad class of elasto-plastic materials the constitutive stiffness matrix can be written as

$$\mathbf{K}^{(\text{const})}=\mathbf{K}^{(e)}+\mathbf{K}^{(p)}(\mathbf{S}), \tag{2.2}$$

where $\mathbf{K}^{(e)}$ is the classical elastic stiffness matrix while $\mathbf{K}^{p}$ is its correction due to plastic effects.

The solution to Eq. (2.1) (advanced incrementally for prescribed load increments and supplemented by the Newton–Raphson iteration scheme) should, up to some numerical accuracy, follow the primary equilibrium path of the exact nonlinear solution for the discretized problem considered. This is so until a singularity point appears at which there is no solution (in the case of the limit point) or the solution is nonunique (in the case of the bifurcation point). The analysis around the critical points on the primary equilibrium path will be referred to as the stability analysis. To by-pass the singularity many algorithms have been proposed in the literature. We could mention in this context:

i) Change of the load-type control of the process into a displacement-type control. The method is effective for limit points only. Also, some complications arise for continuously distributed loads.

ii) Imposing kinematic (buckling mode) constraints at the bifurcation point. The method requires some knowledge of the nature of the postcritical structural behaviour which can be gained either from the corresponding eigenvalue considerations or, in simpler cases, from intuition and engineering experience.

iii) Use of the so-called scalar current stiffness parameter of BERGAN [8] to guide the algorithm suppressing equilibrium iterations.

iv) Use of the "constant-arc-length method" proposed by RIKS [9].

v) Use of the perturbation approach, [10–13], which forms a very general basis for nonlinear calculations but can turn out to be expensive.

vi) Use of the dynamic relaxation method.

vii) Use of the "artificial-spring method", [14].

A highly complicated analysis around the critical points can be sometimes replaced by a simpler, linearized algorithm of the so-called bifurcation theory. According to this approach, the condition for the solution nonuniqueness is given as

$$\det\left[\mathbf{K}^{(e)}+\mathbf{K}^{(p)}(\mathbf{S})+\mathbf{K}^{(\sigma)}(\mathbf{S})+\mathbf{K}^{(u)}(\mathbf{r})+\mathbf{K}^{(R)}(\mathbf{R},\mathbf{r})\right]=0 \tag{2.3}$$

or, after some approximations, as

$$\left\{\mathbf{K}^{(e)}+\mathbf{K}^{(p)}(\sigma^*)+\mu\left[\mathbf{K}^{(\sigma)}(\sigma^*)+\bar{\mathbf{K}}^{(u)}(\mathbf{r}^*)\right]\right\}\mathbf{v}=\mathbf{0}, \tag{2.4}$$

where σ^*, $\mathbf{r}^*$ are certain reference values of the Cauchy stress and the displacement fields, respectively corresponding to the reference external load $\mathbf{R}^*$, $\bar{\mathbf{K}}^{(u)}$ stands

for the linear (in **r**) part of the initial displacement matrix while μ is an unknown multiplier of load for buckling (eigenvalue of the problem (2.4)) and **v** is the corresponding buckling mode (eigenvector). Many effective iterative algorithms are known to handle the eigenvalue problem (2.4); the subspace iteration method was used in the course of the present investigations, [26].

3. Numerical analysis of static instabilities

Numerical illustrations of static instability analyses given in the present paper are basically not meant to propose any new solution algorithms. Instead we would like:

i) to show the class of problems which can be effectively treated by the advanced numerical methods,

ii) to set up the basis for further dynamic considerations, [29]

iii) to supply highly nonlinear solutions for different structural problems which can be used in the future for testing refined solution methods.

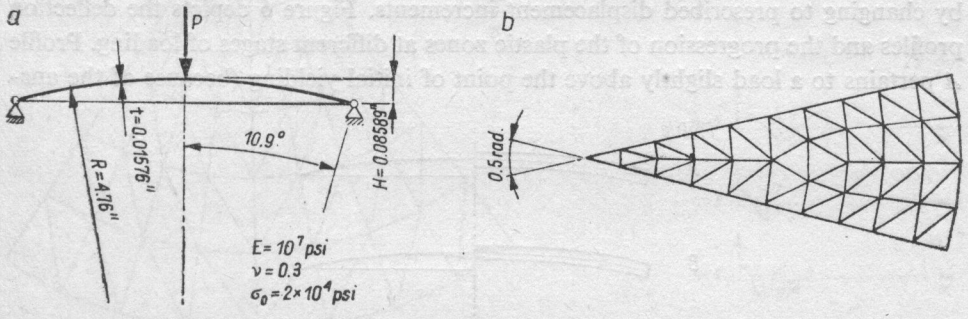

Fig. 4. Shallow spherical can under central load, problem description.

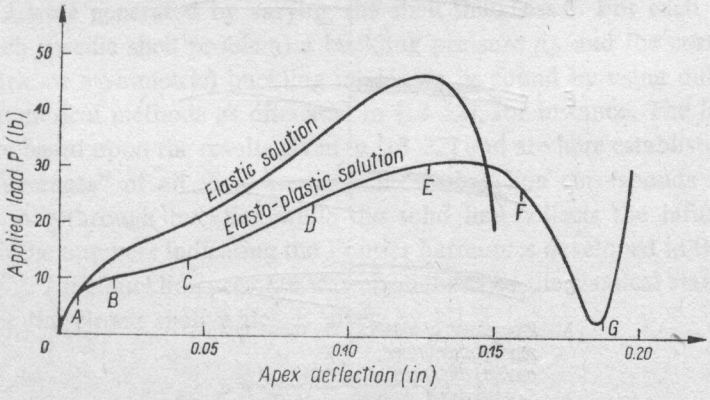

Fig. 5. Shallow spherical cap under central load, load-deflection curve.

As a first example we consider a shallow spherical cap supported at the edge on a fixed hinge circle and subjected to an axial load at the apex, Fig. 4. Both a high precision doubly-curved axisymmetric shell finite element described in [15–17] and the flat triangular shell element TRUMP described in [4] were used for the analysis. At the beginning the fully axisymmetric (one-dimensional) problem was considered. In such a case a wedge-type finite element mesh (Fig. 4) is employed when using TRUMP elements. Figure 5 shows the load-deflection curves of the apex for both the purely elastic and the elasto-ideally plastic cases as well as for both the element types employed. The elasto-plastic response curve shows a pronounced softening region after the shell starts to yield in bending at the apex; this is followed by a stiffening due to membrane action. The load reaches its maximum shortly after the outer portion of the shell—first slightly lifted due to arch action—sinks below its original spherical shape (sign change of the rotation at the support). The load almost reaches its minimum when the edge portion of the shell moves through the horizontal at the support (rotation and original inclination at the support coincide).

The first phase of the response was obtained by applying prescribed load increments. Then, at the instability points, the numerical problems were by-passed by changing to prescribed displacement increments. Figure 6 depicts the deflection profiles and the progression of the plastic zones at different stages of loading. Profile *A* pertains to a load slightly above the point of initial yielding (because of the ana-

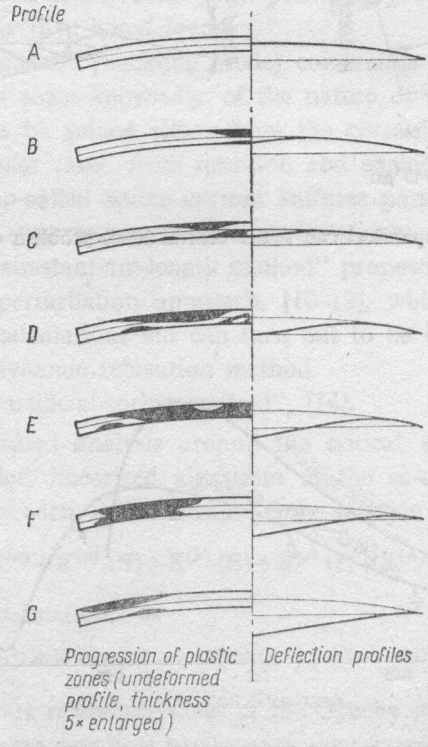

FIG. 6. Shallow spherical can under central load, deflection profiles at different stages of loading.

lysis method employed, plastic flow does not set in immediately as a concentrated force would strictly impose). Profiles B and C clearly demonstrate the reduction of the bending compressive zone at the apex as a consequence of increasing membrane tension. Profile E, shortly below the peak, represents the stage of maximal plastic flow. Profiles F and G show the subsequent drastic unloading, particulary in the inner part of the shell. The response analysis is terminated after plastic flow is renewed at the apex.

As a next step the behaviour of a class of spherical caps clamped at the boundary has been analysed under statically applied uniform external pressure. First, the elastic material properties were considered only. The shell parameter λ defined as, cf. Fig. 4, 7.

$$\lambda = 2\,[3\,(1-\nu^2)]^{1/4}\,(H/t)^{1/2} \simeq [12\,(1-\nu^2)]^{1/4}\,\frac{a}{(Rt)^{1/2}} \tag{3.1}$$

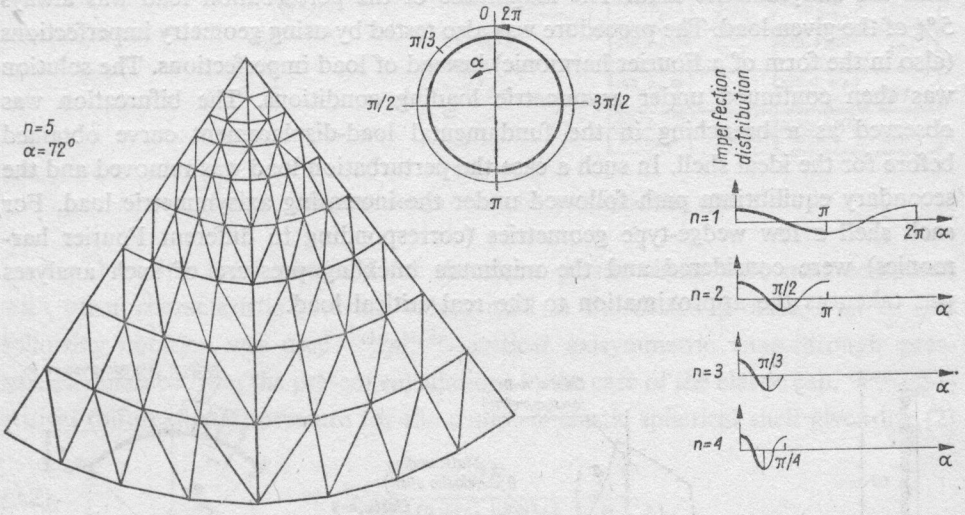

FIG. 7. Analysis of asymmetric deformation modes.

was used to classify different shell problems considered. The different values of the parameter λ were generated by varying the shell thickness t. For each value of λ (e.g. for each specific shell problem) a buckling pressure p_{cr} and the corresponding (axisymmetric or asymmetric) buckling mode can be found by using different analytical or numerical methods as discussed in [18–22], for instance. The lines drawn in Fig. 8 are based upon the results given in [18–22] and are here established as some "weighted averages" of all these results. The broken line corresponds to the axisymmetric snap-through buckling while the solid line collects the bifurcation solutions with the numbers indicating the Fourier harmonics developed in the buckling mode. In Fig. 7 the buckling pressure was normalized by the classical static buckling pressure for the closed shell which is given by [2],

$$p = \frac{2E}{[3\,(1-\nu^2)]^{1/2}} \left(\frac{t}{R}\right)^2. \tag{3.2}$$

The results obtained by the present author and his collaborators are also given in Fig. 7. First, fully axisymmetric analysis was carried out incrementally for elastic shells characterized by $\lambda=8$ and $\lambda=14$. Then asymmetric deformation modes were induced by introducing load and/or geometry imperfections into the shell discretized by means of the triangular elements TRUMP [4]. It was assumed that asymmetric deformation modes were fully represented by a single n-th harmonic mode and the axisymmetric mode. A finite element model for a portion of shell having an angle of π/n was introduced with the element mesh shown in Fig. 7. The symmetry conditions on boundary nodes were introduced in such a manner that the desired harmonic mode (or its multiples) and the axisymmetrical displacements were exactly simulated. The nonlinear load-displacement path was traced up to a certain load without considering harmonic imperfections. To initialize asymmetric deformations at a certain load level a small pressure-type perturbation load was introduced along with the axisymmetric load. The magnitude of the perturbation load was always 5% of the given load. The procedure was also tested by using geometry imperfections (also in the form of a Fourier harmonic) instead of load imperfections. The solution was then continued under asymmetric loading conditions. The bifurcation was observed as a branching in the fundamental load-displacement curve obtained before for the ideal shell. In such a case the perturbation load was removed and the secondary equilibrium path followed under the increasing axisymmetric load. For each shell a few wedge-type geometries (corresponding to different Fourier harmonics) were considered and the minimum buckling pressure of such analyses was taken as the approximation to the real critical load.

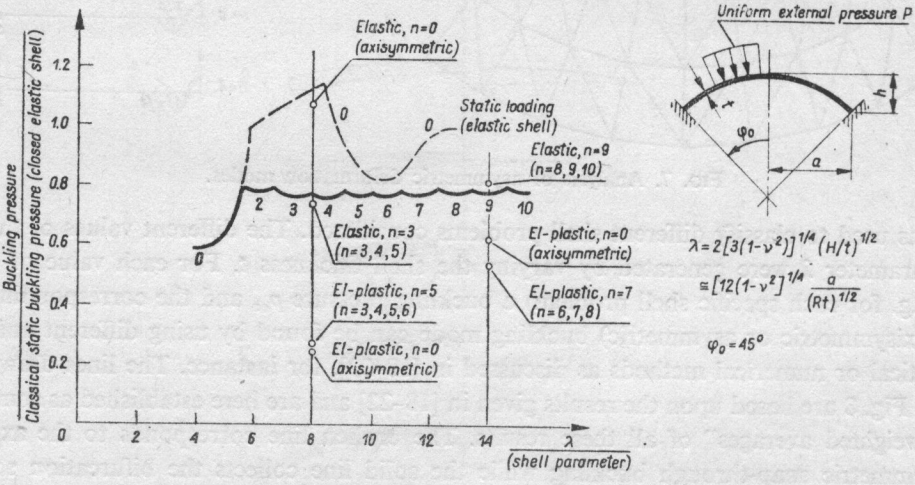

FIG. 8. Static buckling pressures for elastic clamped shallow spherical shells.

In all the cases considered the bifurcation loads were only slightly lower than the following asymmetric snap-through loads. For $\lambda=8$ the critical load value shown in Fig. 8 was chosen between those corresponding to $n=3$, 4 and 5; the

critical pressure obtained for $n=3$ was the lowest. The other results obtained by means of the TRUMP element are also shown in Fig. 8. In the case of elasto-plastic analysis the isotropic hardening of the Ramberg–Osgood type was assumed here, Fig. 9.

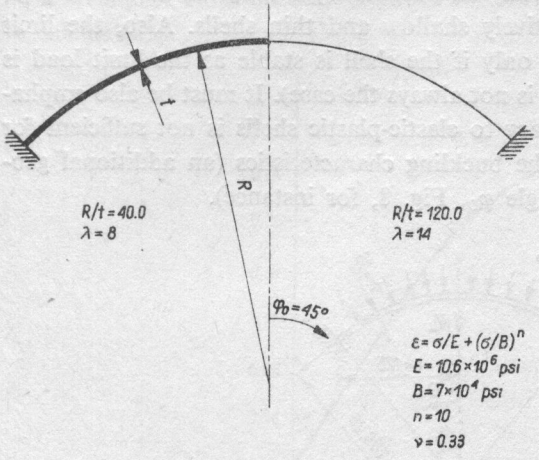

λ=8		λ=14	
	P		P
$^{cap}P_{cr}^{el,ax}$	9120	$^{compl}P_{cr}^{el}$	905
$^{compl}P_{cr}^{el}$	8145	$^{cap}P_{cr}^{el,ax}$	
$^{cap}P_{cr}^{el,a(3)}$	5323	$^{cap}P_{cr}^{el,a(5)}$	706
$^{cap}P_{lim,+}^{e-p}$	2180	$^{cap}P_{lim,+}^{e-p}$	700
$^{compl}P_{cr}^{e-p}$	2135	$^{cap}P_{lim,-}^{e-p}$	700
$^{cap}P_{cr}^{e-p,a(3)}$	1977	$^{cap}P_{cr}^{e-p,ax}$	575
$^{cap}P_{cr}^{e-p,ax}$	1975	$^{compl}P_{cr}^{e-p}$	562
$^{cap}P_{lim,-}^{e-p}$	1900	$^{cap}P_{cr}^{e-p,a(7)}$	506

FIG. 9. Different design loads for two spherical caps.

The buckling loads obtained for the elasto-plastic shells were next compared with other characteristic pressure values used in the design process, Fig. 9. The following notation was used: $^{cap}p_{cr}^{el,ax}$—critical axisymmetric snap-through pressure as obtained from the present calculations in the case of the elastic cap, $^{compl}p_{cr}^{el}$—critical (bifurcational) pressure for the complete elastic spherical shell given by, [2]

$$(3.2)_1 \qquad {}^{com\ l}p_{cr}^{el} = \frac{2E}{[3\,(1-\nu^2)]^{1/2}} \left(\frac{t}{R}\right)^2,$$

$^{cap}p_{cr}^{el,a(3)}$—critical bifurcation ($n=3$) pressure as obtained from the present calculations in the case of the elastic cap, $^{cap}p_{lim,+}^{e-p}$—upper bound to the limit load for the elasto-ideally plastic cap, [23], $^{cap}p_{lim,-}^{e-p}$—lower bound to the limit load for the elasto-ideally plastic cap, [23], $^{compl}p_{cr}^{e-p}$—critical (bifurcational) pressure for the complete elasto-plastic spherical shell given by, [2]

$$(3.3) \qquad {}^{compl}p_{cr}^{e-p} = \frac{4E}{[6\,(1+\nu)\,(1-2\nu+E/E_t)]^{1/2}} \left(\frac{t}{R}\right)^2,$$

E_t is the tangent modulus obtained here assuming the Ramberg–Osgood isotropic hardening of the form shown in Fig. 9, $^{cap}p_{cr}^{e-p,a(5)}$—critical bifurcation ($n=5$) pressure as obtained from the present calculations in the case of the elasto-plastic cap, $^{cap}p_{cr}^{e-p,ax}$—critical axisymmetric snap-through pressure as obtained from the present calculations in the case of the elasto-plastic cap.

To make the problem clearer, the shells geometries shown in Fig. 9 illustrate the real R/t ratios as considered in the numerical analysis. The elasto-plastic buckling results obtained compare well with the results reported in [24].

It must be stressed that the extension of the classical elastic results to a class of elastic-plastic shells is of great practical value as the significance of the elastic shell buckling theories is limited to relatively shallow and thin shells. Also, the limit analysis supplies meaningful results only if the shell is stable as the limit load is reached (which, as seen from Fig. 9, is not always the case). It must be also emphasized that the parameter λ in contrary to elastic-plastic shells is not sufficient for shell classification with respect to the buckling characteristics (an additional geometric parameter is needed—the angle φ_0, Fig. 8, for instance).

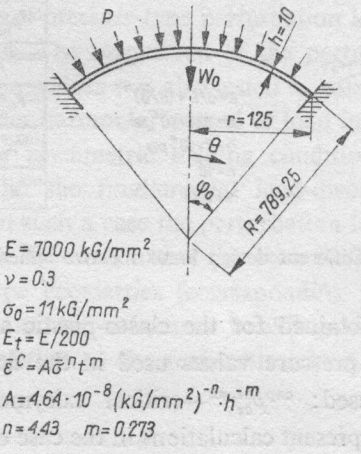

FIG. 10.

As a next example the elasto-plastic-creep analysis of a spherical aluminium cap elamped at the boundary is presented, Fig. 10, [16]. The cap was subjected to the external pressure and analysed incrementally in the elasto-plastic range up to the loss of stability of the snap-through type. The axisymmetric "one-dimensional" finite elements were used so that bifurcation phenomena were automatically excluded. The snap-through instability occurred at $p=26.5$ kG/cm^2. Then the same cap was calculated anew and simulated to creep under the pressure of 25 kG/cm^2 which was 1.5 kG/cm^2 less than the critical value. Assuming the creep law in the form

$$\Delta\boldsymbol{\varepsilon}^{(c)} = \frac{3}{2\bar{\sigma}}\,\Delta\bar{\varepsilon}^{(c)}\,\boldsymbol{\sigma}_{\mathrm{dev}} \tag{3.4}$$

with

$$\Delta\bar{\varepsilon}^{(c)} = A\bar{\sigma}^m t^n \tag{3.5}$$

and the constants A, m, n taken from [25], the results of the numerical analysis are shown in Figs. 11, 12 and 13. The apex displacement versus time curve defines the creep snap-through instability taking place after 1.2 hour of the process. In Fig. 12 the mid-surface displacements are shown for three different moments, the

last one right before buckling Figures 12 and 13 illustrate also the plastic zone development and the distribution of the meridional stresses σ_s. The results were compared with those given in [25]. The qualitative agreement was good while some quantitative differences were attributed to the much simpler finite elements of [25] and a bit higher constant load assumed for creep in the present paper to speed up the calculations.

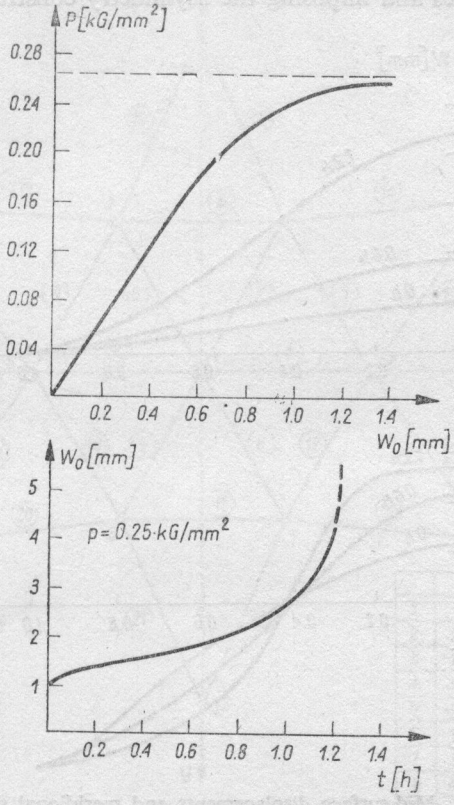

FIG. 11.

As a next example we would like to discuss the static behaviour of a certain space truss structure shown in Fig. 14. For simplicity we exclude in what follows the possibility of local buckling of the truss elements. Let this shell-like structure be loaded by a concentrated force at the apex (or, when needed, by the prescribed vertical displacement at this point). Applying the former and assuming elastic material properties, the incremental analysis was termined at the first limit point L_1, Fig. 15. The calculations were then continued using the prescribed displacement. This was possible until the first bifurcation point (B_1, Fig. 15) was reached. At this point two (or more) equilibrium paths are possible—the first one fully symmetric (fundamental) and the other with certain asymmetry in the deformation pattern. As no eigenvalue analysis was attempted in the course of the truss calculations, we managed to get through the point B_1 by imposing some symmetry constraints

upon the vertical displacements of the truss as described in Fig. 15. By using such constraints we were able to proceed with the incremental analysis up to the point E_1 where an obvious nonuniqueness of the prescribed-displacement problem appeared. So as to have a closer look at the nature of bifurcation points encountered along the fundamental path, imperfection-type analyses were carried out. Assuming first the imperfections in the truss geometry by modifying the initial vertical coordinates of the truss nodes and imposing the asymmetry constraints of the form $w_2 =$

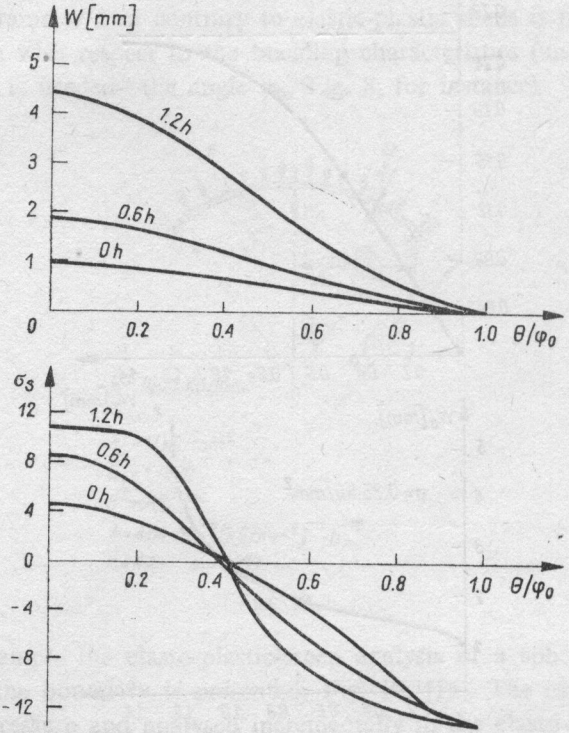

FIG. 12. Mid-surface displacements and meridional stresses.

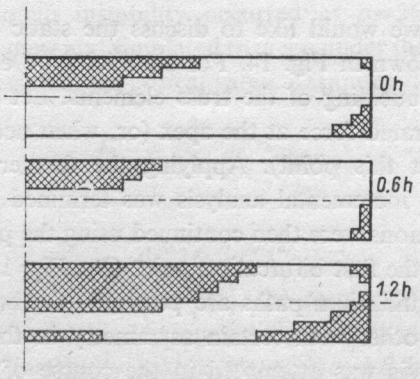

FIG. 13. Plastic zone development in the creeping plate.

$=w_3$, $w_4=w_7$, $w_5=w_6$ (where w_i is the vertical displacement of the i-th nodal point) we discovered this to lead to an unstable post-critical behaviour with the branching point coinciding precisely with the bifurcation point B_1 as found before. Similar analyses allowed to find out the character of all the post-critical equilibrium paths(4). The whole analysis was terminated after reaching some point E_2 at which fully stable behaviour was observed.

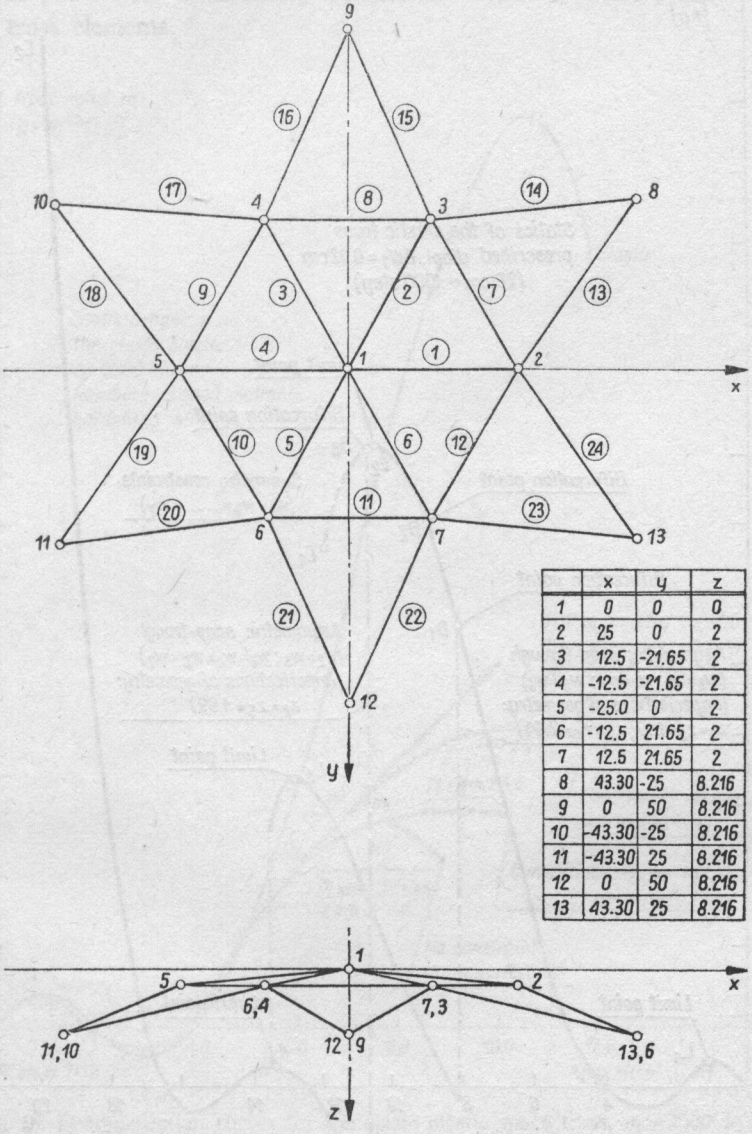

	x	y	z
1	0	0	0
2	25	0	2
3	12.5	-21.65	2
4	-12.5	-21.65	2
5	-25.0	0	2
6	-12.5	21.65	2
7	12.5	21.65	2
8	43.30	-25	8.216
9	0	50	8.216
10	-43.30	-25	8.216
11	-43.30	25	8.216
12	0	50	8.216
13	43.30	25	8.216

FIG. 14. Geometry of space truss.

(4) The nature of the bifurcation point B_2 was not analysed.

We would like to end up this preliminary description of a typical structura behaviour with the remark that even very simple elastic stuctures can be characterized by an extremely complicated load-displacement diagram when full range onlinear behaviour is of interest.

n

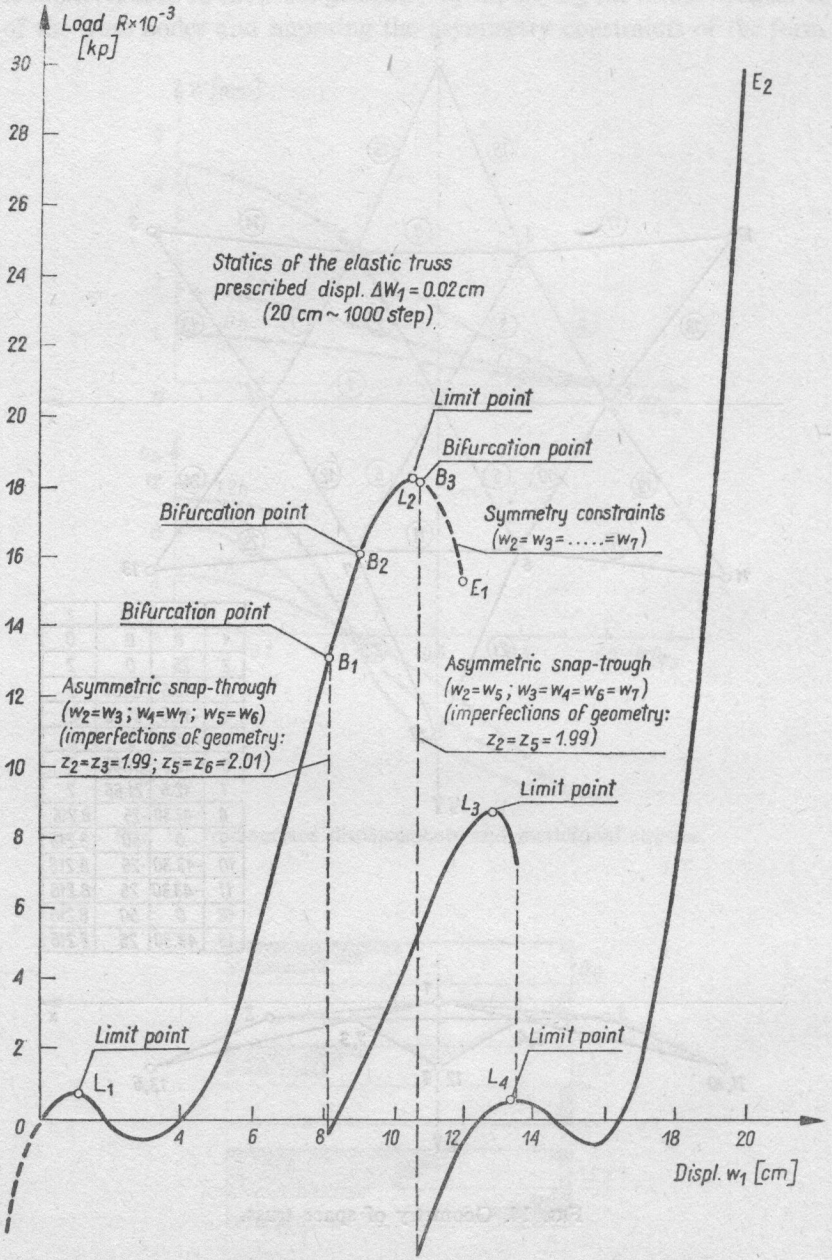

FIG. 15. Load-deflection curves for the elastic space truss, $\sigma_0 = 2000$ kG/cm.^{2}

The similar analyses were carried out assuming elasto-plastic material behaviour of the truss elements. The results obtained for two different yield limits are shown in Figs. 16 and 17 and compared with the fundamental elastic behaviour. In the figures limit and bifurcation points as well as plastified elements at different deformation stages are indicated. The imposed-symmetry approach allows again to characterize the post-critical structural behaviour. Asymmetries of the secondary equilibrium paths were always very distinct and resulted in the plastic unloading of some truss elements.

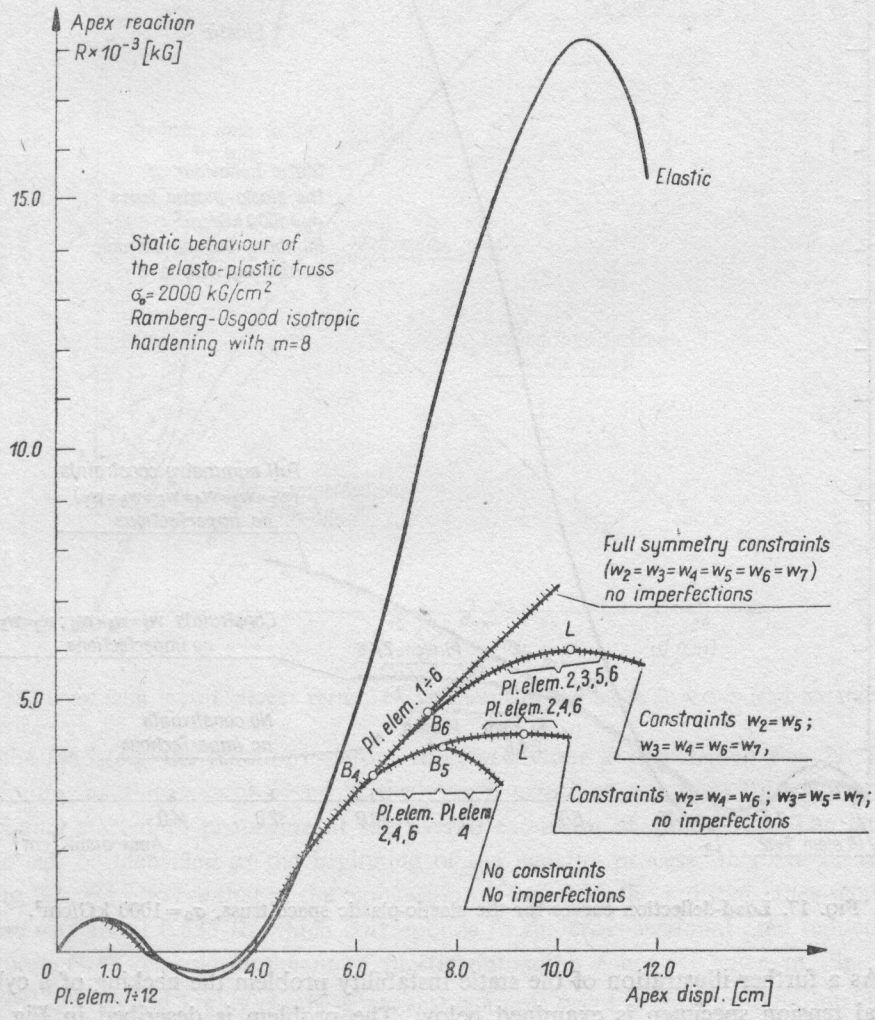

FIG. 16. Load-deflection curves for the elasto-plastic space truss, $\sigma_0 = 2000$ kG/cm².

The same truss structure was next analysed under the set of concentrated forces described in Table 1. The results of the analysis are given in Figs. 18 and 19. Different small geometry and loading imperfection patterns were considered, Table 1.

The results obtained clearly show the essential influence of the imperfections upon the response curve characterizing the ideal problem. The truss under the specific loading considered is said to be imperfection sensitive.

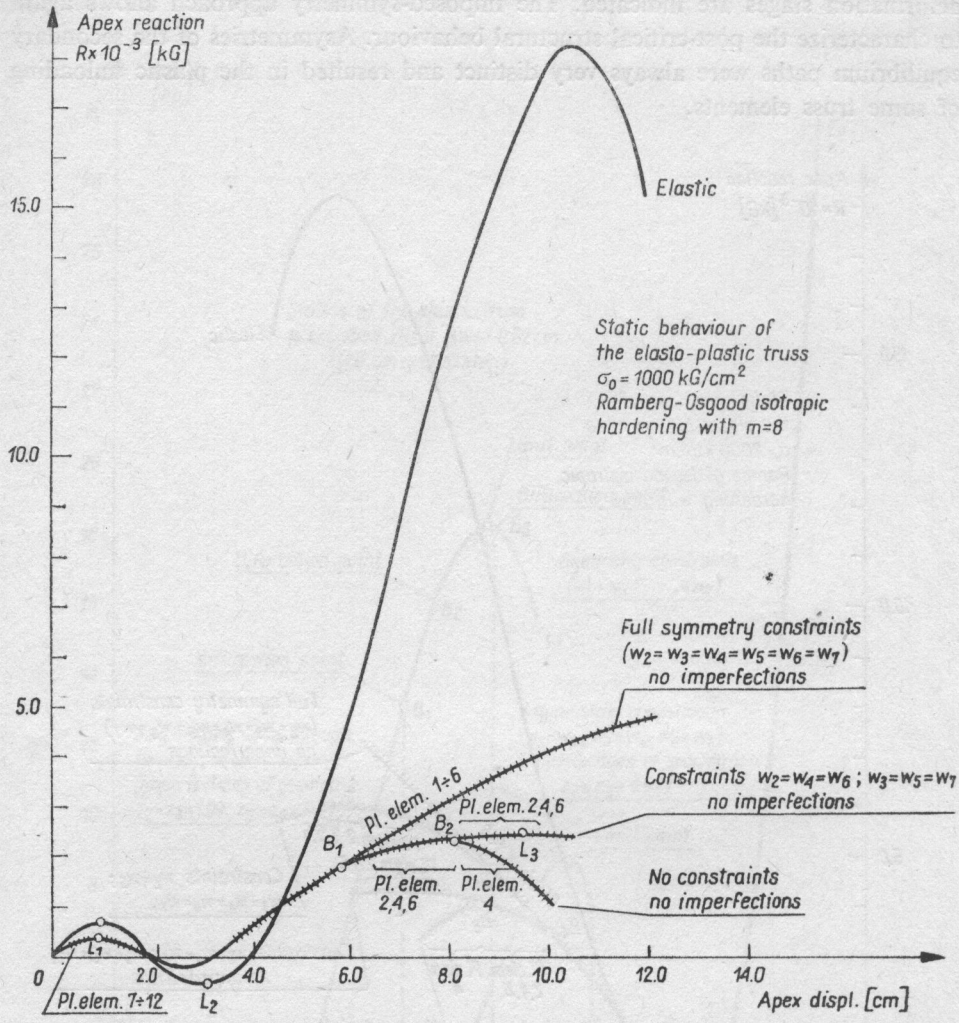

FIG. 17. Load-deflection curves for the elastic-plastic space truss, $\sigma_0 = 1000$ kG/cm^2.

As a further illustration of the static instability problem the necking of a cylindrical tension specimen is examined below. The problem is described in Fig. 20 where the geometrical and material data as well as the mesh lay-out consisting of the axisymmetric TRIAX 3 elements are given. The initial length-to-diameter ratio of the bar is 4. The tensile loading is introduced by the prescribed extension of the end section. The bar was taken to have a reduction in the width at its midlength centerline of 0.005 R so that a standard deformation process might be formulated.

The exact shape of the geometry imperfection is shown in Fig. 20. The magnitude of the incremental extension was taken as $6 \cdot 10^{-4}$ with a final overall stretch ratio of 0.42 (this required 700 prescribed displacement increments).

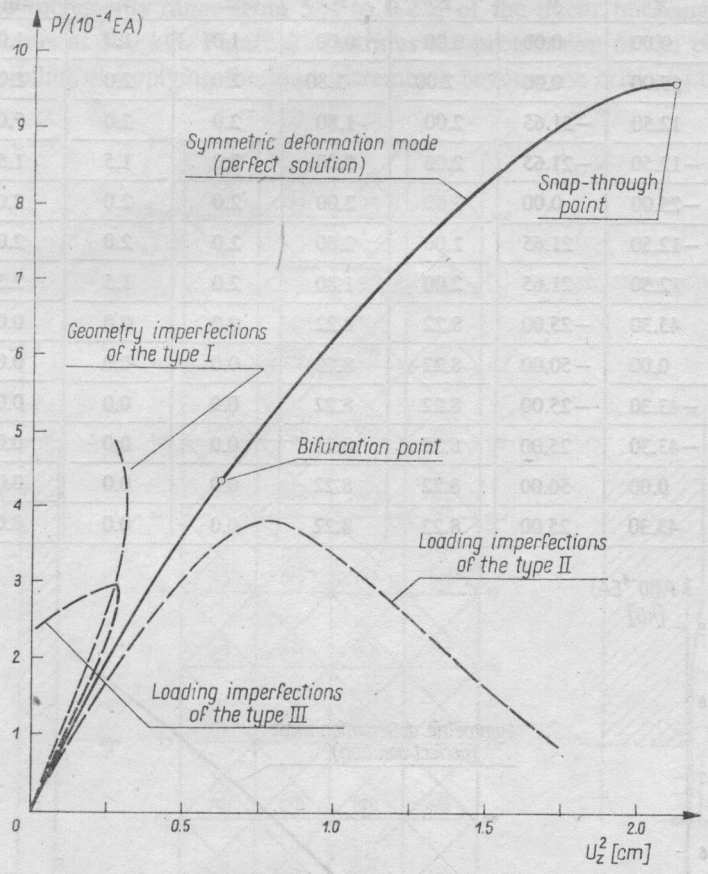

FIG. 18. Truss with imperfections: vertical displacement of the mode 2 versus load parameter.

The load (e.g. the reaction) -deformation behaviour is depicted in Fig. 21. The maximum reaction was observed at the overall extension of about 0.14 while the unloading started to propagate at the overall extension of about 0.16. The latter value can be identified as the beginning of the necking process; this can be seen in Fig. 22. We observe that at the elongation of, say, 0.35 the reduced cross-section radius was about 0.635 R, which corresponds to the cross-sectional area reduction of about 60%. The development of plastic unloading zones is shown in Fig. 23.

An numerically highly cumbersome test example was the elasto-plastic buckling problem of a narrow cantilever beam, solved using the TRUMP shell finite element and described in [4], cf. Fig. 2. The elastic-perfectly plastic material model was assumed. The geometry of the beam as well as the mesh lay-out are shown in Fig. 24. The mesh was refined near the clamped end where extensive plastic flow is expected. Because of linearity at the beginning of the response, cf. Fig. 25, the starting value

Table 1.

Node	Coordinates [cm]				Vertical loading ratios		
	Perfect geometry			Imperfect	Perfect	Imperfect	
	x	y	z	z_1	z	z_{II}	z_{III}
1	0.00	0.00	0.00	0.00	1.0	1.0	1.0
2	25.00	0.00	2.00	1.80	2.0	2.0	2.0
3	12.50	−21.65	2.00	1.80	2.0	2.0	2.0
4	−12.50	−21.65	2.00	2.00	2.0	1.5	1.5
5	−25.00	0.00	2.00	2.00	2.0	2.0	2.0
6	−12.50	21.65	2.00	2.00	2.0	2.0	2.0
7	12.50	21.65	2.00	1.80	2.0	1.5	2.5
8	43.30	−25.00	8.22	8.22	0.0	0.0	0.0
9	0.00	−50.00	8.22	8.22	0.0	0.0	0.0
10	−43.30	−25.00	8.22	8.22	0.0	0.0	0.0
11	−43.30	25.00	8.22	8.22	0.0	0.0	0.0
12	0.00	50.00	8.22	8.22	0.0	0.0	0.0
13	43.30	25.00	8.22	8.22	0.0	0.0	0.0

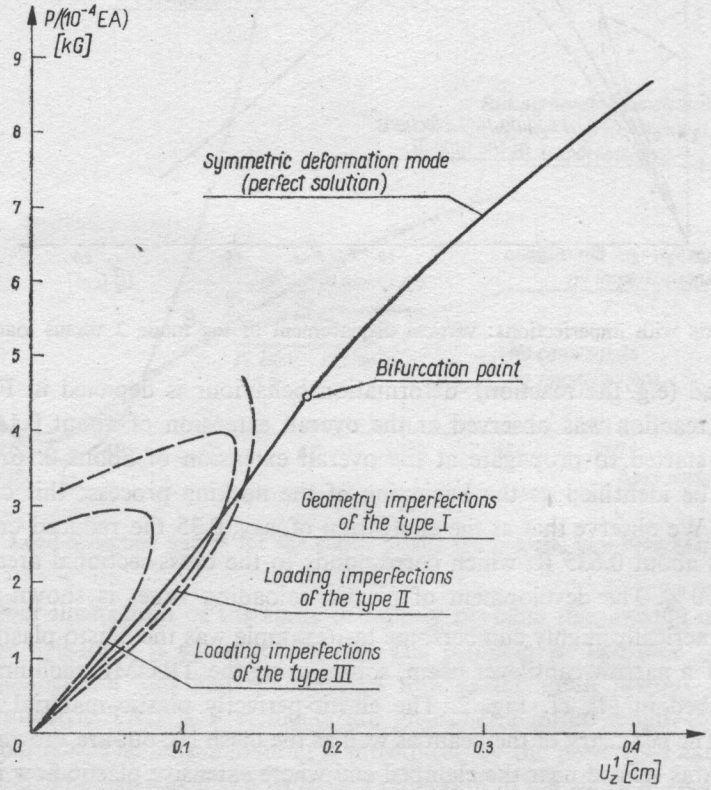

FIG. 19. Truss with imperfections: vertical displacement of the mode 1 versus load parameter.

of the load increment is chosen approximately as 50% of the linear (elastic) buckling load of 1048 kG. A horizontal perturbation load of 0.1% of the vertical load is also acting. Instability arises at a load of about 711 kG. Up to this critical load the applied increments range from 5% to 0.2% of the linear buckling load. First yielding occurs at 530 kG. Figure 2 illustrates the progression of the plastic zones. The imposibility of applying the load increments beyond the critical point imposes

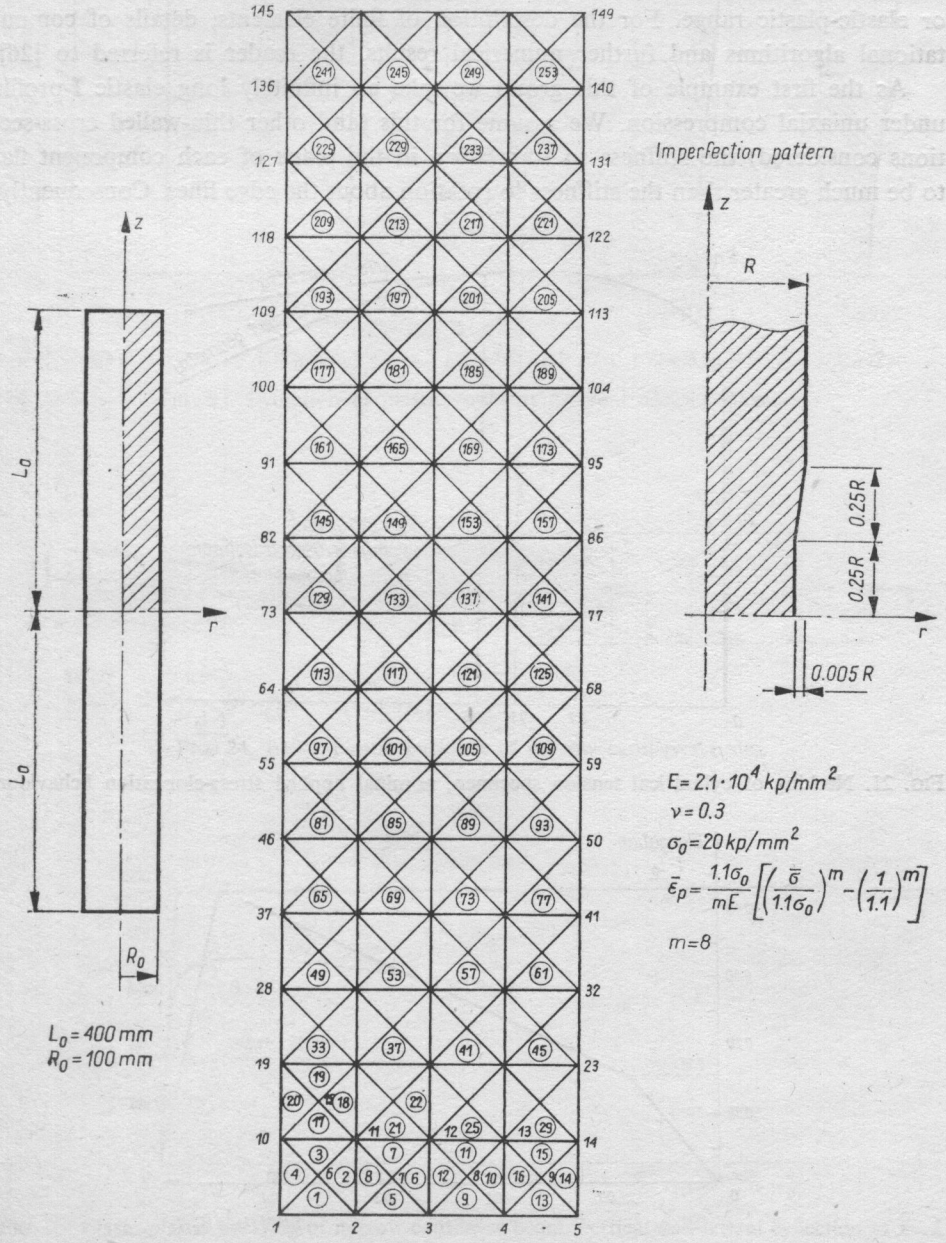

FIG. 20. Cylindrical tension specimen configuration and mesh lay-out.

a change to prescribed displacement increments. The centre of the tip is moved downwards while the perturbation force is gradually taken away. As a consequence of increasing plastic flow which finally covers more than one third of the beam, the lateral bending stiffness of the beam is diminished rapidly.

In order to analyse the effective use of the eigenvalue technique, two examples of the initial structural buckling will now be discussed. We shall illustrate such an approach by considering some prismatic plate assemblies strained into the elastic or elastic-plastic range. For the description of finite elements, details of computational algorithms and further numerical results, the reader is referred to [26].

As the first example of this group we take an infinitely long elastic I-profile under uniaxial compression. We assume for this (and other thin-walled cross-sections considered) the stiffness to translation in the plane of each component flat to be much greater than the stiffness to rotation about the edge lines. Consequently,

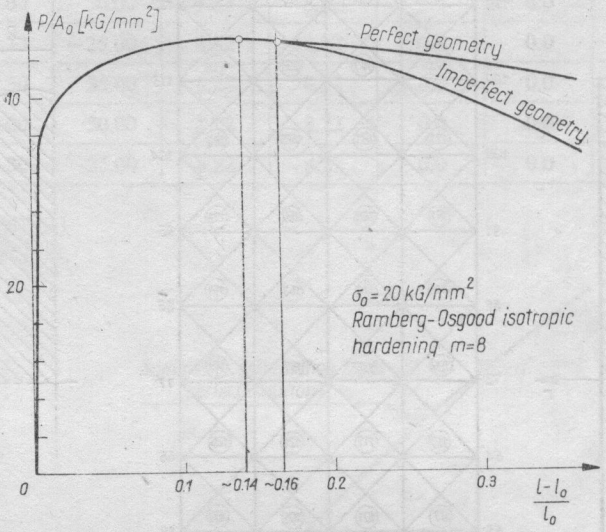

FIG. 21. Necking of cylindrical tension specimen, nominal applied stress-elongation behaviour.

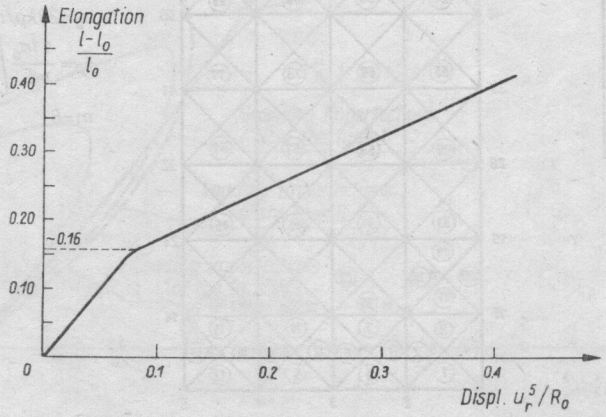

FIG. 22. Reduction of necking section diameter with increasing extension.

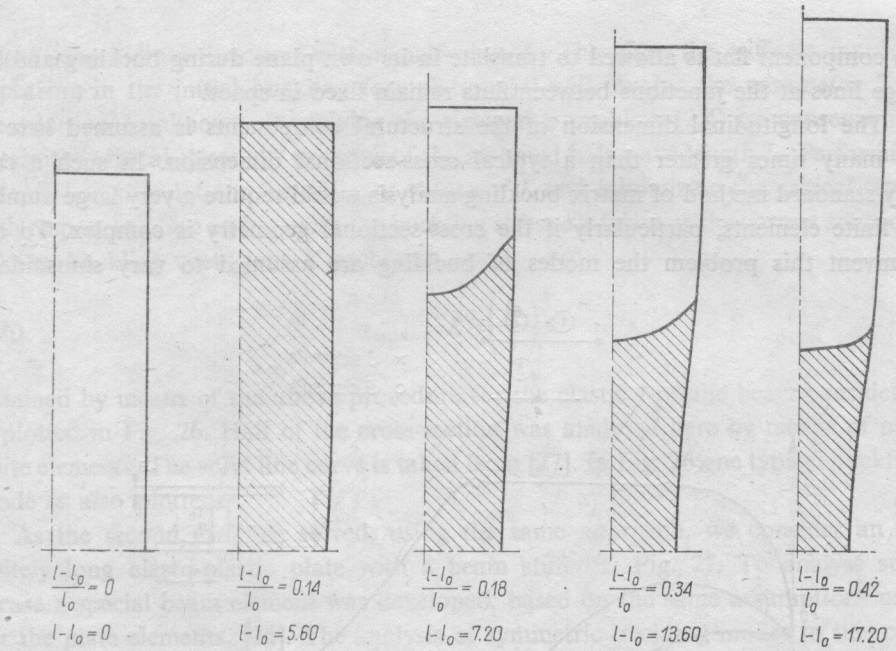

FIG. 23. Evolution of plastic zones at different necking stages.

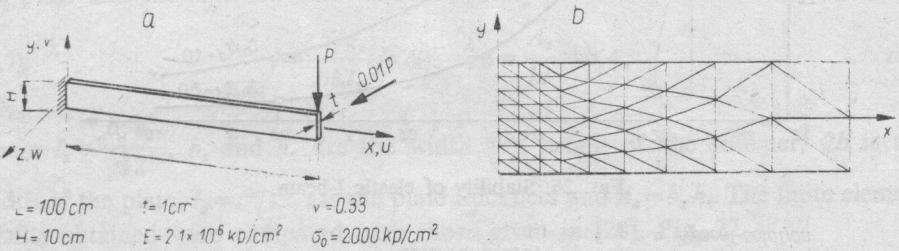

FIG. 24. Elasto-plastic buckling of narrow cantilever beam.

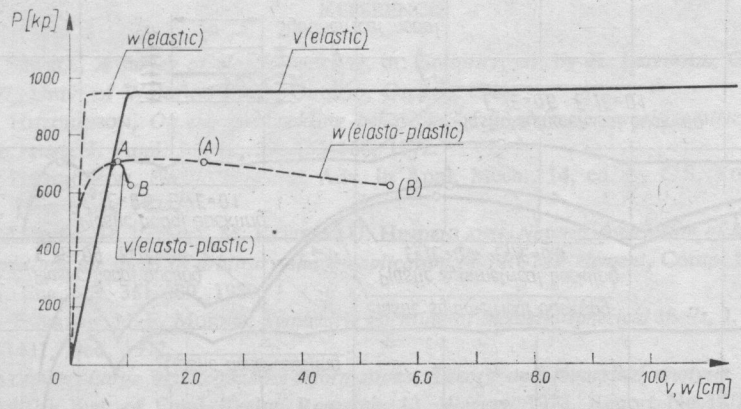

FIG. 25. Elasto-plastic buckling of narrow cantilever beam, vertical and lateral deflection at $x=L$, $y=0$.

no component flat is allowed to translate in its own plane during buckling and the edge lines at the junctions between flats remain fixed in space.

The longitudinal dimension of the structural components is assumed here to be many times greater than a typical cross-sectional dimension. In such a case any standard method of matrix buckling analysis would require a very large number of finite elements, particularly if the cross-sectional geometry is complex. To circumvent this problem the modes of buckling are assumed to vary sinusoidally

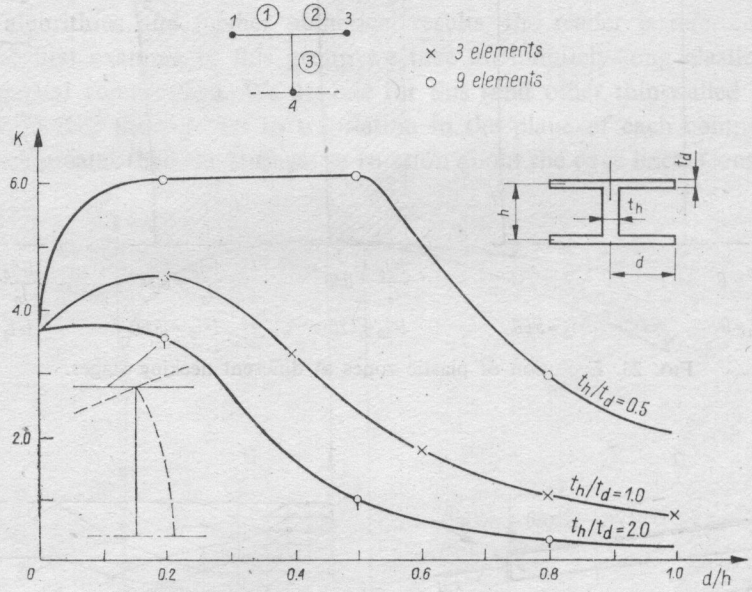

FIG. 26. Stability of elastic I-beam.

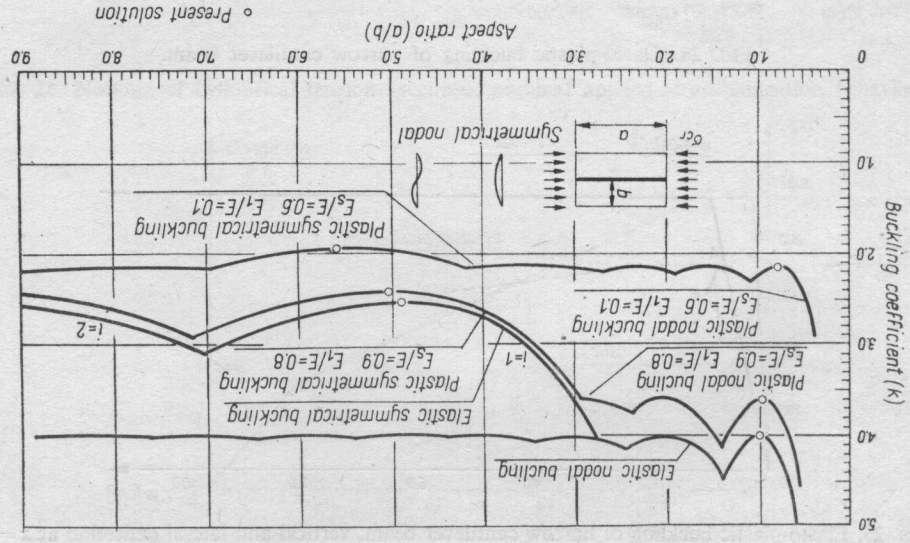

FIG. 27. Stability of elasto-plastic plate with a beam stiffener.

in the longitudinal direction with a half-wave L. Therefore the stiffness matrices appearing in the initial buckling formulation [4] will involve the parameter L as the additional unknown. By solving the eigenvalue problem (2.4) we consequently obtain the critical stress $\sigma_{cr}^{(L)}$ in terms of the assumed half-wave length L. Performing independent calculations for different values of L and minimizing the critical stress with respect to L, we end up with the buckling stress σ_{cr} taken as the correct solution.

The buckling coefficient K such that

$$\sigma_{cr,xx}=KE\left(\frac{t_h}{t}\right)^2 \tag{3.6}$$

obtained by means of the above procedure for the elastic I-profile beam considered is plotted in Fig. 26. Half of the cross-section was analysed here by means of nine finite elements. The solid line curve is taken from [27]. In Fig. 26 one typical buckling mode is also plotted.

As the second example solved, using the same approach, we consider an infinitely long elasto-plastic plate with a beam stiffener, Fig. 27. To analyse such a case a special beam element was developed, based on the same assumptions used for the plate elements, [26]. The analysis of symmetric buckling modes in this case was not possible without the special stiffener element because of the assumption of the fixed edge lines between the flats. The geometry and material properties of the plate and the stiffener were taken to satisfy

$$\gamma=\frac{E_t I_s}{bEI_p}=40, \qquad \delta=\frac{A_s}{bt}=0.4, \tag{3.7}$$

where $I_s=\dfrac{b_s h_s^3}{12}$, b_s and h_s are the width and height of the stiffener, $2b$ is the width of the plate, $I_p=t^3/12$, t is the plate thickness and $A_s=b_s h_s$. The finite element results obtained were compared with those given in [28], Fig. 27.

References

1. M. J. Sewell, *A survey of plastic buckling*, in: *Stability*, ed. by H. Leipholz, Chapt. 5, pp. 85–197, Univ. of Waterloo Press, Ontario, Canada 1975.
2. J. W. Hutchinson, *On the postbuckling behaviour of imperfection-sensitive structures in the plastic range*, J. Appl. Mech., **39**, 155–168, 1972.
3. J. W. Hutchinson, *Plastic buckling*, Adv. in Appl. Mech., **14**, ed. by C.S. Yih, Academic Press, New York 1974.
4. J. H. Argyris, H. Balmer, M. Kleiber, U. Hindenlang, *Natural description of large inelastic deformations for shells of arbitrary shape-application of TRUMP element*, Comp. Meths. Appl. Mech. Eng., 22, 361–389, 1980.
5. N. K. Emerton, N. F. Morris, *Symmetric buckling of inelastic spherical shells*, J. Mech. Div., 1417–1431, Ded. 1972.
6. M. Kleiber, *Large elastic-plastic deformations, Theory and numerical analysis of structures* [in Polish], Inst. of Fund. Techn. Research, 13, Warsaw 1978, Report No 13/1978.
7. M. Kleiber, *Variational formulation in finite deformation elasto-plasticity with large increments and discontinuous fields*, Proc. Int. Conf. on "Variational methods in mechanics", Chicago 1979.

8. P. G. BERGAN *et al.*, *Solution techniques for non-linear finite element problems*, Int. J. Num. Meths. Eng., **12**, 1677–1696, 1978.
9. E. RIKS, *An incremental approach to the solution of snapping and buckling problems*, Int. J. Sol. Struct., **15**, 529–551, 1979.
10. Y. HANGAI, S. KAWANATA, *Perturbation method in the analysis of geometrically nonlinear and stability problems*, Adv. Comp. Meths. in Struct. Mech. and Design, VAH Press, 433–442, Univ. of Alabama, Hunstville 1972.
11. J. J. CONNOR, N. MORIN, *Perturbation techniques in the analysis of geometrically nonlinear shells*, High Speed Computing of Elastic Structures, 683–706, Univ. of Liege 1971.
12. Y. YAKOO, T. NAKAMURA, K. VETANI, *The incremental perturbation method for large displacement analysis of elastic-plastic structures*, Int. J. Num. Meths. Eng., **10**, 503–525, 1978.
13. M. KLEIBER, *Perturbation appsoach to the incremental equations of large deformation elasto-plasticity*, Int. Conf. CAFEM-5: "Computational aspects of the finite element method", Berlin 1979; also: Bull. Acad. Polon. Sci. Série. Sci. techn., **18**, 75-80, 1980.
14. E. W. WRIGHT, E. H. GAYLORD, *Analysis of unbraced multistory steel rigid frames*. Proc. ASCE, J, Eng. Div., **94**, 1143–1163, 1968.
15. M. KLEIBER, *SHELAX—large elasto-plastic deformations of thin shells by the finite element method* [in Polish], Report 49, Inst. of Fund. Technol. Research, Warszaw 1977.
16. W. BORKOWSKI, M. KLEIBER, *Nonlinear statics and dynamics of thin axisymmetric shells by high precision finite elements*, Arch. Mech., 1981 **34**, 15-37, 1982
17. W. BORKOWSKI, M. KLEIBER, *Static and dynamic stability of axisymmetric elastic and elasto-plastic shells* [in preparation].
18. B. O. ALMROTH, E. MELLER, F. A. BROGAN, *Compuer solutions for static and dynamic buckling of shells*, Symp. IUTAM "Buckling of Structures", pp. 52–66, Cambridge, USA 1974.
19. N. AKKAS, N. R. BAULD Jr. *Buckling and post-buckling of spherical caps*, J. Mech. Div., EM3, 727–739, June 1971.
20. R. E. BALL, *A program for the nonlinear static and dynamic analysis of arbitrarily loaded shells of revolution*, Comp. Struct., **2**, 141–162, 1972.
21. N. C. HWANG, *The unsymmetrical buckling of thin shallow spherical shells*, J. Appl. Mech., **31**, 447–457, 1964.
22. R. E. BALL, M. D. SHUTT, *Buckling of shallow spherical, shells—the significance of the pole conditions*, J. Appl. Mech., 46, 710–711, 1979.
23. P. G. HODGE Jr., *Plastic analysis of structures*, McGraw-Hill, New York 1959.
24. L. J. GALLETA, N. F. MORRIS, *Inelastic buckling of spherical shells*, J. Mech. Div. Ang., 795–810, 1974.
25. G. YAGAWA, N. MIYAZAKI, Y. ANDO, *An analysis of elasto-plastic creep buckling of axisymmetric shells by the finite element method*, Arch. Mech., **27**, 869–882, 1975.
26. M. KLEIBER, A. ZACHARSKI, *Numerical analysis of local instabilities in elastic and elastic-plastic prismatic plate assemblies*, Comp. Meths. Appl. Mech. Eng. **31**, 149-168, 1982
27. Royal Aeronautical Society, Structure Data Sheets, 1.
28. H. L. SUJATA, *Plastic buckling of longitudinally stiffened plates*, J. Aerospace Sci., **28**, 1961.
29. M. KLEIBER, *Some results on the numerical analysis of structural instabilities, Part II. Dynamics*. Rozpr. Inż. **30**, 355-367, 1982

STRESZCZENIE

PRZYKŁADY NUMERYCZNEJ ANALIZY NIESTATECZNOŚCI KONSTRUKCJI CZĘŚĆ I. STATYKA

W pracy podano szereg przykładów zastosowania metody elementów skończonych do analizy utraty stateczności sprężystych i niesprężystych układów konstrukcyjnych poddanych obciążeniom statycznym. Omówiono krótko podstawy teoretyczne, koncentrując następnie uwagę na analizie otrzymanych wyników numerycznych.

Резюме

ПРИМЕРЫ ЧИСЛЕННОГО АНАЛИЗА НЕУСТОЙЧИВОСТИ КОНСТРУКЦИЙ
Ч. I. СТАТИКА

В работе приведен ряд примеров применения метода конечных элементов для анализа потери устойчивости упругих и неупругих конструкционных систем, подвергнутых статическим нагрузкам. Кратко обсуждены теоретические основы, концентрируя затем внимание на анализе полученных численных результатов.

POLISH ACADEMY OF SCIENCES
INSTITUTE OF FUNDAMENTAL TECHNOLOGICAL RESEARCH

Received August 13, 1981.